Supporting Information

Peterson et al. 10.1073/pnas.1502742112

SI Text

The β2 adrenergic receptor (β2AR) was originally mutated based on the crystal structure of rhodopsin (1) to yield a β-arrestin biased β2AR termed β2AR-TYY. These residues were mutated in D_2R (Fig. S1*A*); however, robust separation between G-protein and β-arrestin pathways was not achieved. Therefore, EA was used to predict the phenotypes of single point mutations (Table S1). The ET predicted residues (TYY) were mutated to different amino acids, depending on their harshness score. EA was used in four rounds of ET-guided residue determination [mapped to D_3R (2) in Fig. S1*B*] that were carried out with the development of the more complex ET algorithm piET (Fig. S1*C*) and as more detailed crystal structures were solved including the C terminus of $G_{\alpha t}$ in complex with rhodopsin (Fig. S1*D*) (3) and β2AR in complex with $G_{\alpha\beta\gamma}$ (Fig. S1*E*) (4). The four rounds of ET-guided mutagenesis are depicted in a traditional snake-like plot of D_2R in Fig. 1*A* with residues highlighted with the same color scheme as Fig. S1 *A*–*E*. Finally, each point mutation was tested for G protein, β-arrestin, and plasma membrane phenotypes and scored according to their activity profiles (Fig. S2*A*). The mutants that preserved activity at either G protein or β-arrestin were further combined to yield a rich landscape of functionally selective mutants (Fig. S2 *B*–*D*). However, $^{[Gprot]}D_2R$ and $^{[\beta arr]}D_2R$ were chosen from the double point mutants for further characterization because of their robust separation of function and preservation of $^{[WT]}D_2R$'s other major functions (Fig. 2).

SI Materials and Methods

G-Protein Activity. D_2R's ability to inhibit cAMP production was carried out as previously described (5) using the Promega GloSensor assay with minor modifications. D_2R was expressed with 1 μg of DNA and the GloSensor construct was transiently transfected along with 5 μg of D_2R DNA. The luminescence was quantified with the Mithras LB940 instrument with no wavelength filter between the cells and the photomultiplier.

Bioluminescent Resonance Energy Transfer. BRET was performed as previously described (6).

Radioligand Binding. [^{3}H]-raclopride (Promega) binding was carried out as previously described (7).

ERK Phosphorylation by Western Blot. HEK 293T cells were transiently cotransfected with 2.5 μg of mutant D_2Rs or pcDNA (for untransfected control) and 1 μg of either pcDNA or β-arrestin 2-YFP (the same BRET construct). After 24 h, cells were starved in serum-free DMEM, and 24 h later, cells were stimulated with 1 μM quinpirole for 10 min. Then cells were lysed in ice-cold RIPA buffer containing protease and phosphatase inhibitor mixtures (Sigma). Lysates were blotted for p-ERK (Cell Signaling Technology, #9106) and total ERK (Cell Signaling Technology, #9102).

Receptor Internalization Assay. All D_2R constructs have an N-terminal triple HA-tag, and internalization was performed as previously described (8). Percent internalization was determined from unstimulated receptor expressing cells.

Confocal Microscopy. HEK 293T cells were transiently transfected with YFP C-terminally tagged to D_2R and plated onto 5% fibronectin treated glass bottom culture dishes. The cells were cultured and imaged as previously described (9) with minor modifications. Cells were cultured for 24 h post transfection, and images were captured on live cells.

MAP Kinase Transcriptional Activity Reporter. The SRF and SRE transcriptional reporter was assessed as previously described (10) with minor modifications. The cells were transfected using the calcium phosphate method described here, with 1 μg of D_2R DNA and 5 μg of SRF or SRE reporter DNA. Finally, the cells were incubated in serum-free DMEM overnight rather than using serum replacement medium.

Adeno-Associated Viral Expression Vectors. The triple HA-D_2R constructs had NheI and AscI sites cloned onto the 5′ and 3′ end of D_2R, respectively. This construct was ligated into the NheI and AscI sites of the pAAV-EF1a-DIO EYFP construct provided by the laboratory of Karl Deisseroth. The YFP was replaced with D_2R.

Adeno-Associated Virus Production. The constructs were packaged into pseudotyped AAV 2/10 using the triple-transfection technique, as previously described (11), which produces helper free virus. The titer was determined to be $\sim 1 \times 10^{13}$ vector genome copies per mL for each virus.

Mouse Stereotaxic Injection for Viral Delivery. Mice were anesthetized under 1–2% isoflurane, and the coordinates from bregma for striatal viral deliver were AP = +1.1 mm, ML = ±1.7 mm, and DV = −2.9 mm for dorsal and −4.0 mm for ventral striatum. 0.75 μL of virus was injected into each site, for a total volume of 3 μL per mouse. The mice were allowed to recover for 2–4 wk, and then behavioral experiments were performed.

Locomotor Activity. The Accuscan activity monitor (Omnitech Electronics, Inc.) was used to assess locomotor activity, as previously described (7).

HA Staining of Virally Transduced Brains. Transduced brains were fixed by perfusion of the mouse and left overnight in 4% PFA in PBS. 30 μM sections were collected by vibratome sectioning and stained by free-floating in 0.3% triton-X in PBS supplemented with 2% NGS and 3% BSA. The HA antibody (3724; Cell Signaling) was diluted 1:1,000 and allowed to incubate overnight.

1. Shenoy SK, et al. (2006) beta-arrestin-dependent, G protein-independent ERK1/2 activation by the beta2 adrenergic receptor. *J Biol Chem* 281(2):1261–1273.
2. Chien EY, et al. (2010) Structure of the human dopamine D3 receptor in complex with a D2/D3 selective antagonist. *Science* 330(6007):1091–1095.
3. Scheerer P, et al. (2008) Crystal structure of opsin in its G-protein-interacting conformation. *Nature* 455(7212):497–502.
4. Rasmussen SG, et al. (2011) Crystal structure of the β2 adrenergic receptor-Gs protein complex. *Nature* 477(7366):549–555.
5. Allen JA, et al. (2011) Discovery of β-arrestin-biased dopamine D2 ligands for probing signal transduction pathways essential for antipsychotic efficacy. *Proc Natl Acad Sci USA* 108(45):18488–18493.
6. Masri B, et al. (2008) Antagonism of dopamine D2 receptor/beta-arrestin 2 interaction is a common property of clinically effective antipsychotics. *Proc Natl Acad Sci USA* 105(36):13656–13661.
7. Urs NM, Snyder JC, Jacobsen JP, Peterson SM, Caron MG (2012) Deletion of GSK3β in D2R-expressing neurons reveals distinct roles for β-arrestin signaling in antipsychotic and lithium action. *Proc Natl Acad Sci USA* 109(50):20732–20737.
8. Espinoza S, et al. (2011) Functional interaction between trace amine-associated receptor 1 and dopamine D2 receptor. *Mol Pharmacol* 80(3):416–425.
9. Snyder JC, Rochelle LK, Lyerly HK, Caron MG, Barak LS (2013) Constitutive internalization of the leucine-rich G protein-coupled receptor-5 (LGR5) to the trans-Golgi network. *J Biol Chem* 288(15):10286–10297.

10. Evron T, et al. (2014) G Protein and β-arrestin signaling bias at the ghrelin receptor. *J Biol Chem* 289(48):33442–33455.

11. Xiao X, Li J, Samulski RJ (1998) Production of high-titer recombinant adeno-associated virus vectors in the absence of helper adenovirus. *J Virol* 72(3):2224–2232.

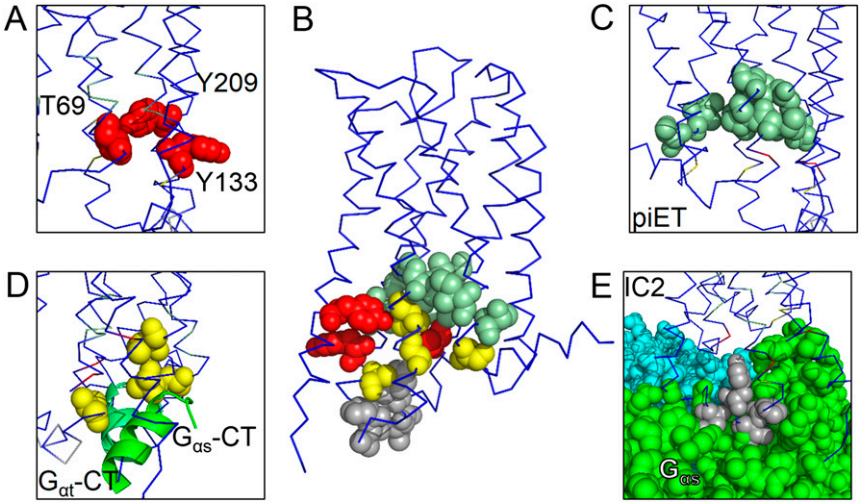

Fig. S1. Evolutionary Trace of D_2R facilitated by advances in crystallography and algorithm design. (*A*) TYY mapped onto D_3R (2) (PDB ID 3PBL in red). (*B*) Four rounds of ET predicted residues for mutagenesis mapped onto D_3R. (*C*) piET (green residues depicted as spheres). (*D*) Gα-CT proximity (3) (PDB ID 3DQB residues in yellow; Gα-CT is represented as a green α-helix cartoon) and (*E*) $G_{\alpha\beta\gamma}$ (4) (PDB ID 3SN6 α is green and β is blue) interaction with IC2 of D_3R (gray spheres).

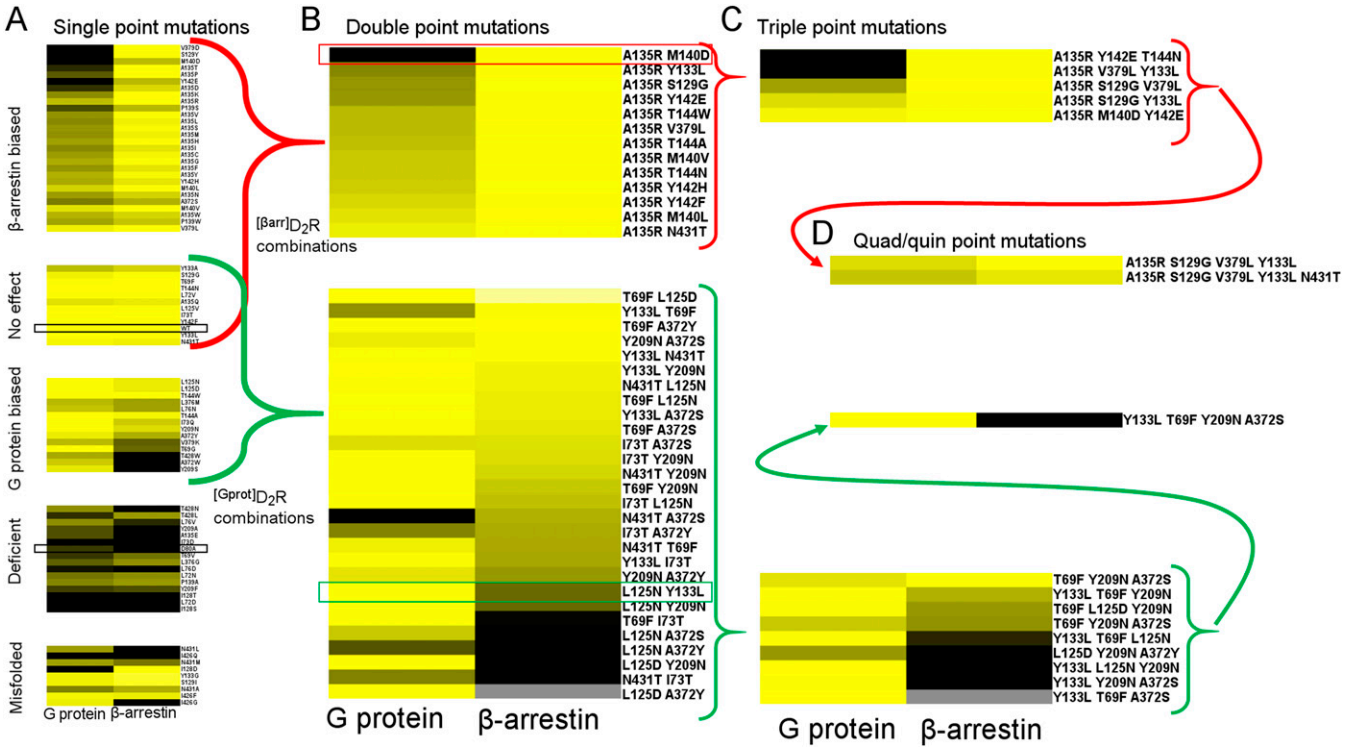

Fig. S2. G-protein and β-arrestin activity of ET predicted mutants. Dose–response curves for each mutant were normalized to a WT control that was performed the same day and the $\log(\tau/K_A)$ was calculated. Because all values were normalized to WT, $\tau = 1$ and $K_A = 1$ for WT; thus, 0 is depicted as yellow, and −3 (100 log fold shift in τ/K_A) is depicted as black in the heat maps. (*A*) G-protein and β-arrestin activity of single point mutations generated mutants that were misfolded, mutants that were biased toward G protein or β-arrestin, or mutants that had little to no effect on any tested function. (*B*) Mutations that had no effect on the desired pathway (red lines for β-arrestin and green for G protein) were combined into double point mutations and (*C*) triple and (*D*) quadruple and one quintuple. The mutations that are further characterized in Fig. 2 are highlighted in boxes.

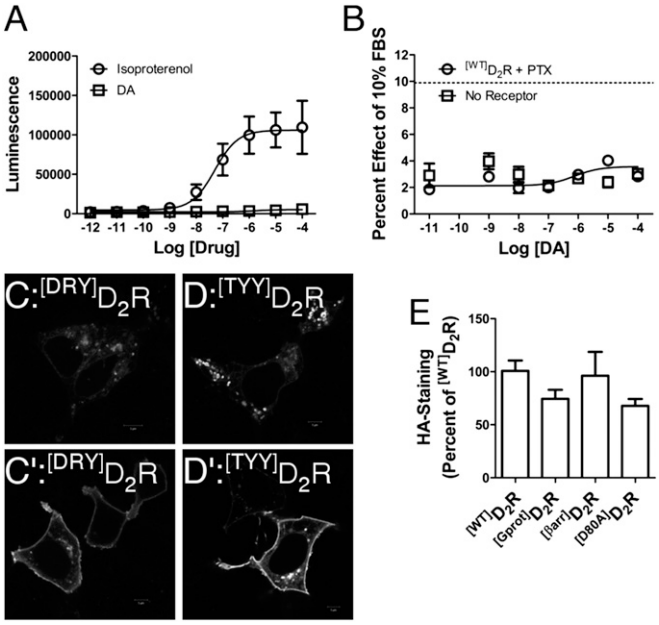

Fig. S3. (*A*) GloSensor response to agonists on endogenous receptors. (*B*) SRF transcriptional activity on endogenous receptors and $^{[WT]}D_2R$ when pertussis toxin is present. $^{[WT]}D_2R$ E_{MAX} (Fig. 3*A*) is represented as a dotted line. Plasma membrane localization deficiencies in mutant receptors (*C*) DRY motif mutated to AAY and (*D*) T69F Y133G Y209A are rescued to the plasma membrane by 24 h treatment with the D_2R antagonist spiperone (*C′* and *D′*, respectively). (*E*) Relative receptor expression levels as determined by HA staining for internalization data presented in Fig. 2*J*.

Table S1. Evolutionary Action-guided mutagenesis

Residue	Color in Fig. 1 and Fig. S1	Predicted residues
T69	Red	GVF
Y133	Red	LAG
Y209	Red	NSFA
A135	Yellow	CSGV
	Yellow	TMPI
	Yellow	LFYN
	Yellow	WQHR
	Yellow	EKD
A372	Yellow	SYW
L376	Yellow	GM
N431	Yellow	AMLT
L72	Green	VND
I73	Green	TQD
L76	Green	VND
L125	Green	VND
I128	Green	TSD
S129	Green	GYI
V379	Green	LDK
I426	Green	FQG
T428	Green	NLW
P139	Gray	ASW
M140	Gray	LVD
Y142	Gray	FHE
T144	Gray	ANW

Each residue predicted from ET (first column) is color coded the same in Fig. 1 and Fig. S1 (colors indicated in the second column). The third column shows the predicted residues in increasing ET harshness (amino acid conservation and side chain chemistry) from left to right. Each single point mutation was generated and tested for G-protein and β-arrestin activity. Note that A135 was found to be a critical residue for G-protein activation but not β-arrestin activation, and all 19 mutations were made to titrate the most β-arrestin biased mutant.

Table S2. Calculated values from Figs. 2 and 3

Assay	$^{[WT]}D_2R$	$^{[Gprot]}D_2R$	$^{[\beta arr]}D_2R$	$^{[D80A]}D_2R$
cAMP E_{MAX}, % of WT	100 ± 6.9	103 ± 7.1	49 ± 15	28 ± 16
cAMP EC_{50}, nM	6.6 ± 1.6	8.4 ± 1.5	7,000 ± 3,000	18,000 ± 12,000
β-arrestin E_{MAX}, % of WT	104 ± 4.0	15 ± 7.0	88 ± 3.3	−3.0 ± 5.4
β-arrestin EC_{50}, nM	41 ± 1.0	360 ± 92	6.2 ± 0.1	39 ± 32
K_I of DA, nM	810 ± 10	260 ± 10	310 ± 10	1,100 ± 100
Internalization % of surface D_2R	29 ± 2.5	8.4 ± 3.1	26 ± 3.1	3.4 ± 2.7
Internalization EC_{50}, nM	510 ± 10	47 ± 16	830 ± 10	410 ± 40
SRF E_{MAX}, % of FBS	7.8 ± 1.0	5.8 ± 0.9	−0.2 ± 0.2	Not converged
SRF EC_{50}, nM	90 ± 2.0	32 ± 2.0	250 ± 200	Not converged
SRE E_{MAX}, % of FBS	5.6 ± 1.8	4.2 ± 1.4	Not converged	1.3 ± 0.8
SRE EC_{50}, nM	35 ± 5.0	8.0 ± 12	Not converged	0.09 ± 0.03